ACS OMEGA

Open Access

http://pubs.acs.org/journal/acsodf

Article

Optical Analysis Method for Turbid Media Based on Wedge-Shaped Cells at Different Angles

Zhe Zhao, Ruina Zhu, Yuyan Yang, Huiquan Wang,* Jinhai Wang, and Guang Han

Cite This: *ACS Omega* 2024, 9, 18119−18126

Read Online

ACCESS | Metrics & More | Article Recommendations

ABSTRACT: The wedge-shaped sample cell, by offering a comprehensive representation of scattering information in turbid media, significantly enhances the informational content conveyed by spectral images compared to flat sample cells. To further refine the accuracy of turbid medium component detection utilizing wedge-shaped sample cells, this work undertakes modeling and analysis of the influence of different wedge angles on detection precision. In this study, employing a 5° gradient in the incident angle of light, we investigate the impact of incident angles ranging from 10 to 45° on the turbid medium component analysis. Validation experiments are performed by utilizing solutions of Indian ink and fat emulsion at varying ratios. Experimental findings demonstrate that under identical experimental conditions, the wedge-shaped sample cell model at an incident angle of 35° yields optimal analysis results. Utilizing partial least-squares regression (PLSR) for the corresponding optical parameters, the highest value of R_p reached 0.980, with an RMSEP of 0.002. When compared to the model with a 30° incident angle, R_p increased by 0.033, and RMSEP decreased by 0.008. In comparison to the flat sample cell model, R_p increased by 0.041, and RMSEP decreased by 0.004. This study, through continuous variation of wedge angles and PLSR modeling and prediction, further enhances the accuracy of turbid medium component detection, laying an experimental foundation for subsequent analysis of turbid medium components based on wedge-shaped sample cells.

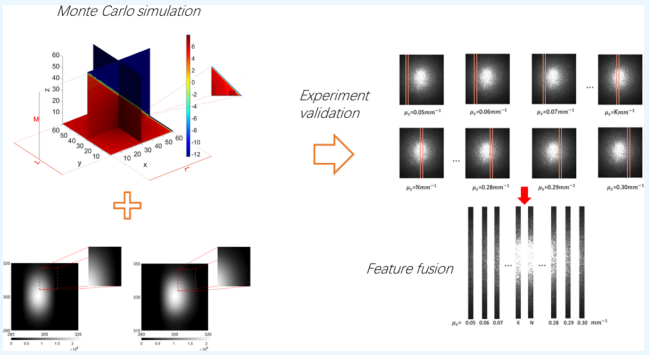

1. INTRODUCTION

Turbid media encompass a variety of solutions exhibiting strong scattering properties, including bacterial suspensions, where the classic Lambert−Beer law encounters limitations in fully describing all of the characteristics of such media. In traditional methods for multicomponent analysis of turbid media, the emphasis has predominantly rested on absorption effects while striving to mitigate or minimize the influence of scattering effects. For example, Kohl et al. introduced a reference wavelength method, wherein solute concentration is increased to elevate the absorption coefficient while concurrently reducing the reduced scattering coefficient.[1] This strategy aims to neutralize absorption and scattering effects in turbid media at a specific wavelength.[2] Horstmeyer et al. have utilized wavefront shaping techniques to manipulate the propagation direction and focal position of light beams, thereby circumventing scattering in biological tissues.[3] These approaches seek to alleviate the impact of scattering effects, facilitating research predominantly focused on absorption effects. However, they do not specifically isolate or analyze scattering information from turbid media. Modeling and analyzing absorption and scattering coefficients in turbid media separately present challenges, and achieving high precision in such analyses can prove to be challenging.

The presence of scattering effects leads to photon traveling distances far greater than the thickness of the sample, rendering traditional flat plate models inadequate for addressing the research requirements concerning complex solution-related component information. Consequently, in recent years, scholars have explored scattering information from multiple dimensions including light path, wavelength, and spatial detection position. Zhang and colleagues employed visible and near-infrared transmittance spectroscopy to detect hemoglobin concentration in blood products, accomplishing multiple path length analysis without compromising the integrity of the blood bag.[4] Their study established a regression model utilizing the light intensity−path length slope curve spectrum and hemoglobin concentration, resulting in a correlation coefficient of 0.972 for the prediction set, thus demonstrating the feasibility of multiple path length trans-

Received: December 17, 2023
Revised: February 9, 2024
Accepted: February 20, 2024
Published: April 10, 2024

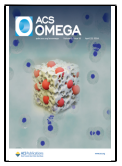

https://doi.org/10.1021/acsomega.3c09525
ACS Omega 2024, 9, 18119−18126

mission for turbid media analysis. Aulbach and others devised techniques for controlling light transmission through opaque scattering media in both spatial and temporal dimensions, enabling precise control over light transmission in such media.[5] This method generates ultrashort pulses from light passing through strongly scattering media, allowing for the manipulation and optimization of pulse duration within the sample. Consequently, this enables the selection of light path length through the medium, thereby achieving modulation in the multiple path length dimension.

However, existing methods for acquiring scattering information from turbid media often entail invasiveness and are characterized by slow processes. Hence, our research team proposed the utilization of a wedge-shaped sample cell[6] to expand the dimensions of path length and facilitate multiple detection positions, thereby enabling noninvasive multiple path length detection. It was observed that employing a wedge-shaped sample cell resulted in differences in the output light spot through the turbid medium compared with traditional detection methods. First, the presence of scattering effects in the turbid medium caused a shift in the peak of the obtained light spot.[7] Second, the varying pathlengths within the wedge-shaped sample cell led to the output light spot no longer being circularly symmetric but axisymmetric along one direction.[8] Characteristics of the light spot are extracted through methods such as contour extraction, elliptical fitting,[9] multidimensional spectral information fusion, and gray-level co-occurrence matrices. The variations in these features precisely depict the expression of scattering information in turbid media.

Based on previous research from our group,[6−9] the wedge-shaped sample pool, due to the nonperpendicular direction of the light source incident to the transmission surface, results in varying path lengths of light propagation in the solution. The thickness of the sample pool also affects the analysis accuracy of complex solution components. This multilight path characteristic is directly reflected in the tilt angle of the sample pool (i.e., the angle of incident light). However, because the optimal light path length obtained at different wavelengths is different, current actual measurements cannot satisfy the requirement that all wavelengths can achieve the optimal light path length. Additionally, there has not been a systematic study to determine the optimal incident light angle for the wedge-shaped sample cell that maximizes the utilization of its multipathlength property for the best representation of scattering information. Therefore, this study explores the propagation patterns of photons in wedge-shaped models at different incident light angles. By comparing the performance of models at different incident light angles, we aim to identify the optimal incident light angle that maximizes the utilization of scattering information contained in the transmitted light spot. The goal is to establish more precise and robust regression models, ultimately enhancing the accuracy of the turbid medium component analysis.

2. MATERIALS AND METHODS

2.1. Models of photon propagation behavior at different wedge angles. This study investigated the propagation behavior of light in wedge-shaped models with different incident angles using Monte Carlo simulation.[10,11] Building upon the GPU-accelerated Monte Carlo simulation method proposed by Fang et al., we modified the boundary conditions to establish a wedge-shaped sample cell model and simulate photon transport at various tilt angles. First, a square with a side length (L) of 60 mm was defined as the photon incident surface, with the photon emission point located at coordinates (30, 30, and 0 mm) on the incident surface. Second, a plane intersecting with the incident surface was set as the transmission surface, and the angle (α) between the two planes was the parameter to be varied, achieved by controlling the side length (M). Then, three additional sides perpendicular to the incident surface and transmission surface were created, forming a fully enclosed wedge-shaped sample cell model. Finally, optical parameters corresponding to the turbid medium were assigned within the model to investigate the photon propagation behavior in turbid media at different wedge angles. The model is illustrated in Figure 1.

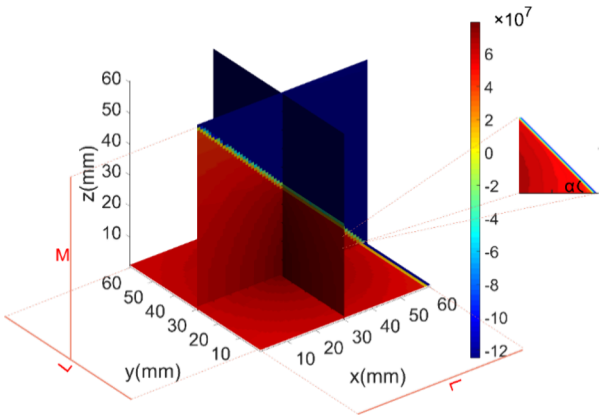

Figure 1. Wedge-shaped sample model based on Monte Carlo simulation.

In this study, Monte Carlo simulations were conducted on turbid media with scattering coefficients ranging from 0.05 to 0.3 mm^{-1}, absorption coefficients ranging from 0.01 to 0.05 mm^{-1}, an anisotropy factor of 0.01, and a refractive index of 1.37. During the simulations, the values of n and g remained constant, while μ_s and μ_a were sequentially varied by using a controlled variable approach. A total of 10^8 photons were emitted, with incident light angles changing in 5° increments from 10 to 45°. Considering the various factors that can introduce errors in real experiments, such as environmental errors, system errors, and random errors, white noise was added to the output light spot on the transmission surface of the wedge-shaped sample cell in this study. This addition aimed to simulate the effectiveness of the model under real experimental conditions.

2.2. Study on the Propagation Behavior of Light in Turbid Media. Under pure absorption conditions, the propagation of light in the sample follows Lambert−Beer's law, that is, the intensity of the emitted light is proportional to the absorbance, the concentration of the measured liquid, and the thickness of the sample. If a traditional flat plate model is used, then a circularly symmetric light spot will be collected. Although a two-dimensional image is obtained, it actually contains only one-dimensional information. Using a wedge-shaped Monte Carlo simulation with varying angles, it was found that due to the presence of scattering effects, the distance traveled by photons in the measured liquid is far greater than the thickness of the measured liquid. This causes the light spot distribution on the transmission surface to be noncircularly symmetric. As the angle increases, the shape of the light spot on the transmission surface will gradually tend to

https://doi.org/10.1021/acsomega.3c09525
ACS Omega 2024, 9, 18119−18126

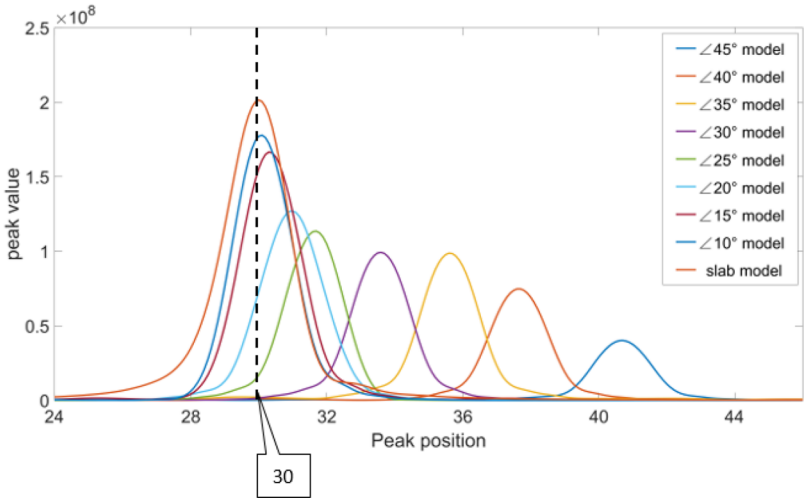

Figure 2. Shift of the light spot peak at different incident angles.

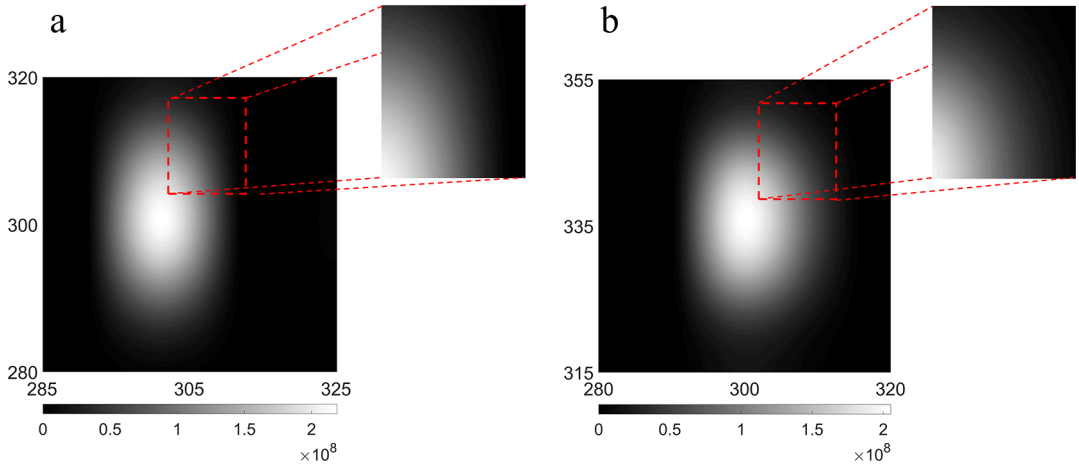

Figure 3. Light intensity distribution on the transmission surface at different incident angles. (a) Light spot image obtained on the transmission surface at 10° incident angle. (b) Light spot image obtained on the transmission surface at 30° incident angle.

be elliptical; the area will continue to increase, and the edges will gradually blur. As the angle changes, the peak of the light spot transmitted through the turbid medium will continuously shift, as shown in Figures 2 and 3. This allows the scattering and absorption effects in the turbid medium to be expressed simultaneously.

2.3. Optimal Tilt Angle of the Wedge-Shaped Sample Cell. As the incident angle of the incident light continuously varies, the shift in the peak value, alteration of shape, and distinct texture features of the transmitted surface light spot are indicative of the expression of scattering information within turbid media. To investigate the angles at which the aforementioned characteristics maximize the representation of scattering properties within turbid media, this study employs a controlled variable approach to sequentially simulate the absorption coefficient within the range of 0.01 to 0.05 mm^{-1} and the scattering coefficient within the range 0.05 to 0.3 mm^{-1}. Initially, the absorption coefficient is set at 0.05 mm^{-1}, resulting in 26 different scattering coefficient values and the corresponding transmitted surface light spot images. With the increase in incident angle, the number of data points on the transmitted surface continuously increases. To standardize the data dimensions for input into the regression model, the 26 light spot images are cropped to a size of 600 × 600. Given the relatively large volume of data and significant redundancy, in order to reduce computational complexity while including as much light spot information transmitted through the turbid medium as possible, 26 columns of data containing the light spot information are selected with the maximum light intensity value at the center.

The study selected the ith column in sequential order from the 26 light spot images, each corresponding to different scattering coefficients, where i ranged from 288 to 313. The 26 columns of data are combined to obtain data of size 600 × 26 dimensions, as shown in Figure 4 and eq 1.

$$X_{\mu_s}^{\theta_i} = \{x_{\mu_{s_1}}^{\theta_i}, x_{\mu_{s_2}}^{\theta_i}, \ldots, x_{\mu_{s_n}}^{\theta_i}\} \quad (1)$$

where $X_{\theta_i}^{\mu_s}$ is the input sample data, μ_{s_n} represents the nth images under different scattering coefficients, and θ_i is the ith column of data under angle θ.

Subsequently, the scattering coefficient is controlled to be 0.2 mm^{-1}, and the light spot images of the transmitted light spots under different absorption coefficients are processed according to the above method, as shown in eq 2.

$$X_{\mu_a}^{\theta_i} = \{x_{\theta_i}^{\mu_{a_1}}, x_{\theta_i}^{\mu_{a_2}}, \ldots, x_{\theta_i}^{\mu_{a_n}}\} \quad (2)$$

https://doi.org/10.1021/acsomega.3c09525
ACS Omega 2024, 9, 18119−18126

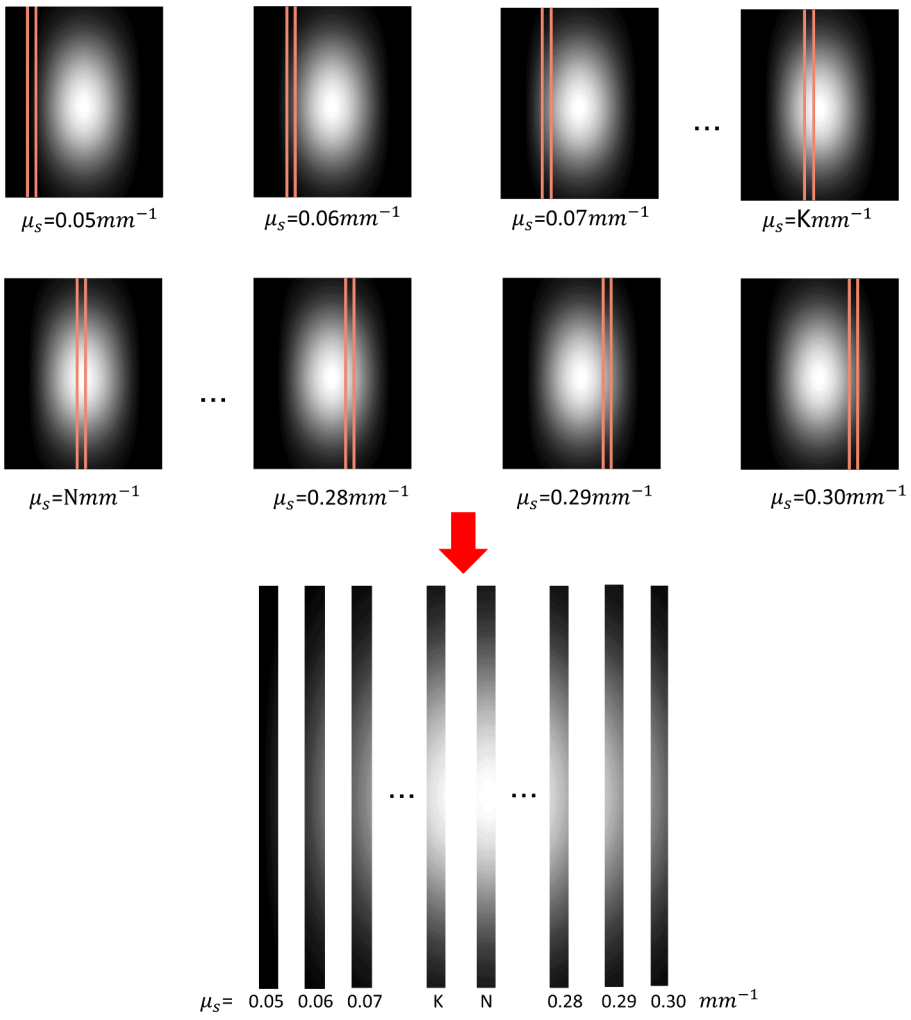

Figure 4. Processing method for light spot data obtained from Monte Carlo simulations of the transmitted surface.

where $X_{\theta_i}^{\mu_a}$ is the input sample data, μ_{a_n} represents the nth images under different absorption coefficients, and θ_i is the ith column of data under angle θ.

Partial least-squares regression (PLSR) was employed to establish a regression model between the light spot data and the corresponding optical parameters. PLSR is widely utilized in near-infrared light spot component analysis.[12,13] PLSR is a multivariate regression modeling method for multiple dependent variables and multiple independent variables, which can better address situations with limited sample sizes. The model performance was evaluated using the correlation coefficient (R_c) and root-mean-square error of calibration (RMSEC) for the modeling data set, as well as the correlation coefficient (R_p) and root-mean-square error of prediction (RMSEP) for the prediction data set. The regression results are presented in Tables 1 and 2, with data dimensions of 26 × 600.

Combining the results from Tables 1 and 2, at an incident angle of 35°, the regression for the scattering coefficient based on the transmitted surface light spot images yielded an R_p value of 0.9718, with the minimum RMSEP being 0.0136. For the regression of the absorption coefficient based on the transmitted surface light spot images at the same incident angle, the $R_p$value reached 0.9863, and the minimum RMSEP was 0.0015.

Table 1. Regression Results of Wedge Models With Different Incident Angles for the Scattering Coefficient in Turbid Media

α	R_c	RMSEC (%)	R_p	RMSEP (%)
10°	0.9975	0.0035	0.8009	0.0360
15°	0.9999	0.0005	0.8169	0.0345
20°	0.9999	0.0008	0.9684	0.0143
25°	0.9999	0.0008	0.9633	0.0155
30°	0.9871	0.0081	0.9539	0.0174
35°	0.9994	0.0017	0.9718	0.0136
40°	0.9874	0.0080	0.9617	0.0158
45°	0.9883	0.0077	0.9647	0.0152

Taking into account the above simulation results, this study concludes that the regression results for both the scattering and absorption coefficients are optimal at an incident angle of 35°. Compared to other incident angles, the light spot images obtained at 35° contain a richer set of component information. This finding identifies the optimal angle for maximizing the expression of the component information and establishes a theoretical foundation for future research.

2.4. Experimental Design. To validate the theoretical research mentioned above, an experimental verification system was designed and constructed. The experimental data collection system for this study was composed of the following

https://doi.org/10.1021/acsomega.3c09525
ACS Omega 2024, 9, 18119−18126

Table 2. Regression Results of Wedge Models for the Absorption Coefficient in Turbid Media at Different Incident Angles

α	R_c	RMSEC (%)	R_p	RMSEP (%)
10°	0.9998	0.00010	0.7588	0.0064
15°	0.9998	0.00014	0.9751	0.0021
20°	0.9997	0.00014	0.9804	0.0018
25°	0.9998	0.00014	0.9785	0.0019
30°	0.9995	0.00026	0.9723	0.0022
35°	0.9995	0.00024	0.9863	0.0015
40°	0.9995	0.00026	0.9693	0.0023
45°	0.9996	0.00021	0.9741	0.0021

components: a 785 nm single-wavelength laser (FL-785−100-M-B, MAX-RAY PHOTONICS) as the light source, an industrial line scan camera (MV-CA020−20GM, HIK VISION), a wedge-shaped sample chamber, an experimental platform, a computer, and the relevant cables, as depicted in Figure 5. During the experimental process, the laser emitted light perpendicular to the incident surface of the wedge-shaped sample chamber, while the camera captured light spot images by positioning itself vertically above the transmitted surface of the wedge-shaped sample chamber.

2.4.1. Sample Preparation. The experimental samples were prepared by blending distilled water, Indian ink, and a fat emulsion in specific ratios. Following the controlled variable method, solutions were prepared with absorption coefficients ranging from 0.02 to 0.07 mm^{-1} and scattering coefficients ranging from 0.14 to 0.39 mm^{-1}. To correspond with the simulation experiments, 26 sets of samples with different absorption coefficients and 26 sets with different scattering coefficients were prepared.

In one set of experiments, the concentration of fat emulsion was kept constant at 1.05 mL, while the concentration of Indian ink varied in a stepwise manner within the range of 0.0008 to 0.0031 mL. In another set of experiments, the concentration of Indian ink was fixed at 0.0022 mL, and the concentration of fat emulsion varied in a stepwise manner within the range of 0.14 to 0.39 mL. These experiments were conducted to validate three different models: the 35° incident angle model, the 30° incident angle model, and the flat plate model. In total, 156 sets of samples were prepared and used in the experiments.

2.4.2. Data Imaging Acquisition. During the experimental process, the prepared solutions were introduced into the wedge-shaped sample chamber. Subsequently, the laser was activated with the laser parameters appropriately configured for laser emission. Data acquisition was controlled with a frame rate of 11 frames per second (fps) and an exposure time of 0.03 s. In each individual experiment, a sequence of 20 photographs was recorded continuously and stored. Upon completion of each individual experiment, the laser was turned off, and the sample chamber was thoroughly cleaned with anhydrous ethanol. This procedure was repeated iteratively, until all experiments were completed.

2.4.3. Data Processing. The data acquired from the experiments were cropped to focus on the region of interest (ROI). Initially, the light spot images were cropped to a size of 1300 × 1040 pixels. To reduce light intensity noise, an average of the 20 images obtained in each individual experiment. Then, the data from the selected ROIs were fused.

To achieve this, with an initial control of the absorption coefficient at 0.05 mm^{-1}, 26 different scattering coefficient values were used to generate transmitted surface light spot images. To include as much light spot information as possible transmitted through the turbid medium, 26 columns of data were selected with the maximum light intensity value as the central point. The 26 light spot images were sequentially used to select the mth column, each corresponding to different scattering coefficients, where m ranged from 400 to 425. The selected 26 columns of data were combined, resulting in a data set with dimensions of 1300 × 26, as illustrated in Figure 6.

Following this process, the scattering coefficient was adjusted to 0.2 mm^{-1}, and the same methodology was applied to process the transmitted surface light spot images with 26 different absorption coefficient values.

3. RESULTS AND DISCUSSION

In this study, the acquired light spot data were utilized to model the corresponding optical parameters through partial least squares regression (PLSR). Initially, the processed light spot images for the 35° incident angle, 30° incident angle, and flat plate model were subjected to PLSR regression to model the scattering coefficient. Subsequently, the obtained regression coefficients were compared. The results are presented in Table 3.

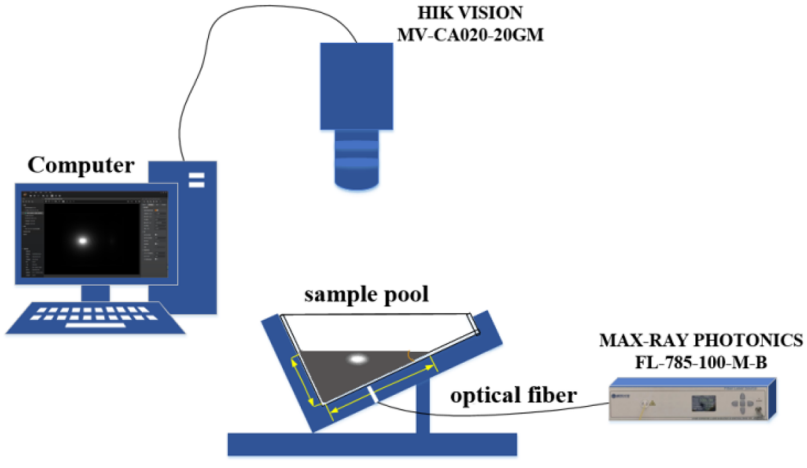

Figure 5. Experimental data collection system.

https://doi.org/10.1021/acsomega.3c09525
ACS Omega 2024, 9, 18119−18126

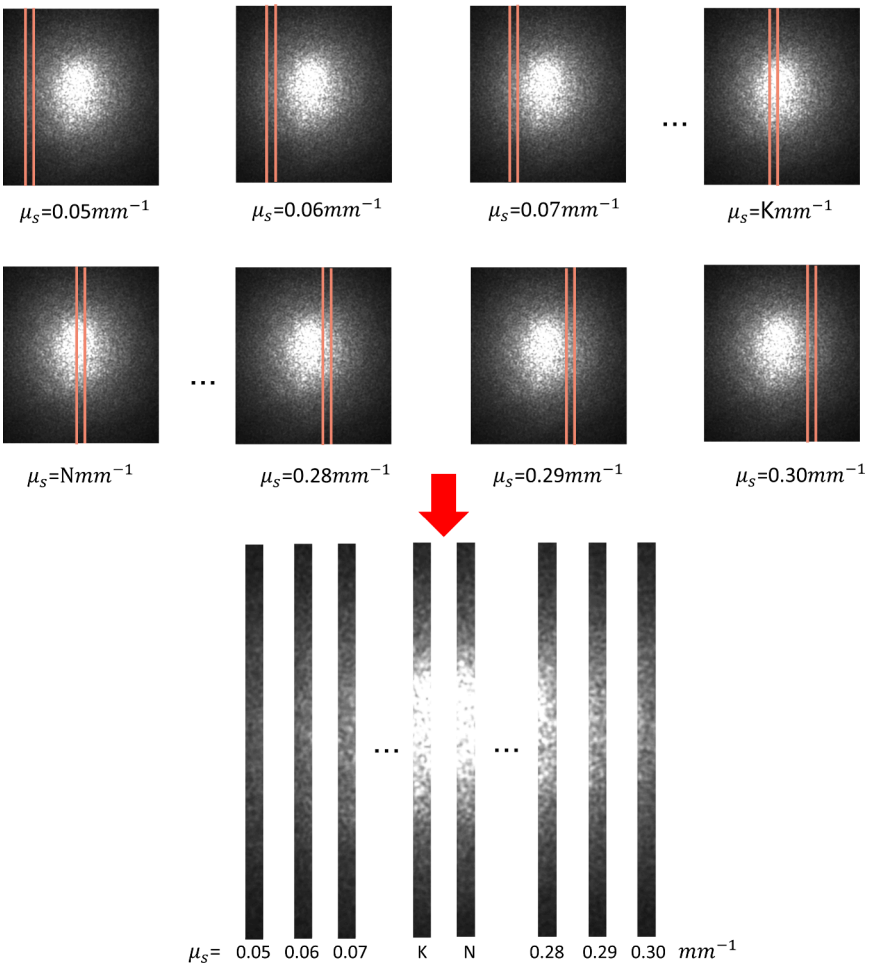

Figure 6. Processing method for the experimental light spot images.

Table 3. Comparison of the Regression Results for Scattering Coefficients Using Light Spot Images Obtained from 35° Incident Angle, 30° Incident Angle, and Flat Plate Models

α	data dimensions	R_c	RMSEC (%)	R_p	RMSEP (%)
30°	26 × 1300	0.9942	0.0054	0.9452	0.0192
35°	26 × 1300	0.9454	0.0171	0.9779	0.0112
slab model	26 × 1300	0.9697	0.0135	0.9372	0.0156

As shown in Table 4, it can be observed that the regression results for the absorption coefficient are most favorable at a 35° incident angle. Specifically, the R_p value reaches 0.9800, with a RMSEP of only 0.0023. Compared to the 30° incident angle model, R_p increased by 0.0097. In contrast to the flat plate model, the R_p at a 35° incident angle has improved by 0.0268,° and the RMSEP has decreased by 0.0004.

Table 4. Comparison of the Absorption Coefficient Modeling Results Based on 35° Incident Angle, 30° Incident Angle, and Flat Plate Models

α	data dimensions	R_c	RMSEC (%)	R_p	RMSEP (%)
30°	26 × 1300	0.9980	0.0006	0.9703	0.0022
35°	26 × 1300	0.9776	0.0021	0.9800	0.0023
slab model	26 × 1300	0.9947	0.0011	0.9532	0.0027

These results indicate that the regression performance for both the absorption and scattering coefficients is notably superior for the 35° incident angle model compared with the other two models. The light spot images obtained at a 35° incident angle contain more component information than the other two models, effectively increasing the information dimensions of the light spot images. Consequently, this further enhances the accuracy of the component analysis in turbid media.

To visually illustrate the superiority of the model at a 35° incident angle, the study displayed the fitting results of training and prediction data sets for the scattering and absorption coefficients obtained through regression using light spot images acquired at 35°, 30°, and flat plate models. This is depicted in Figure 7. In the figure, the horizontal axis represents the actual values of the scattering and absorption coefficients for the training and prediction data sets during regression, while the vertical axis represents the predicted values for both the training and prediction data sets.

From the graph, it can be visually observed that at a 35° incident angle, both the training and prediction values for the regression of the scattering and absorption coefficients are closer to the true values compared to the other two models. This suggests that the 35° incident angle model better represents the absorbing and scattering substances in turbid media and effectively translates the scattering information in turbid media into useful input information. Furthermore, it

https://doi.org/10.1021/acsomega.3c09525
ACS Omega 2024, 9, 18119−18126

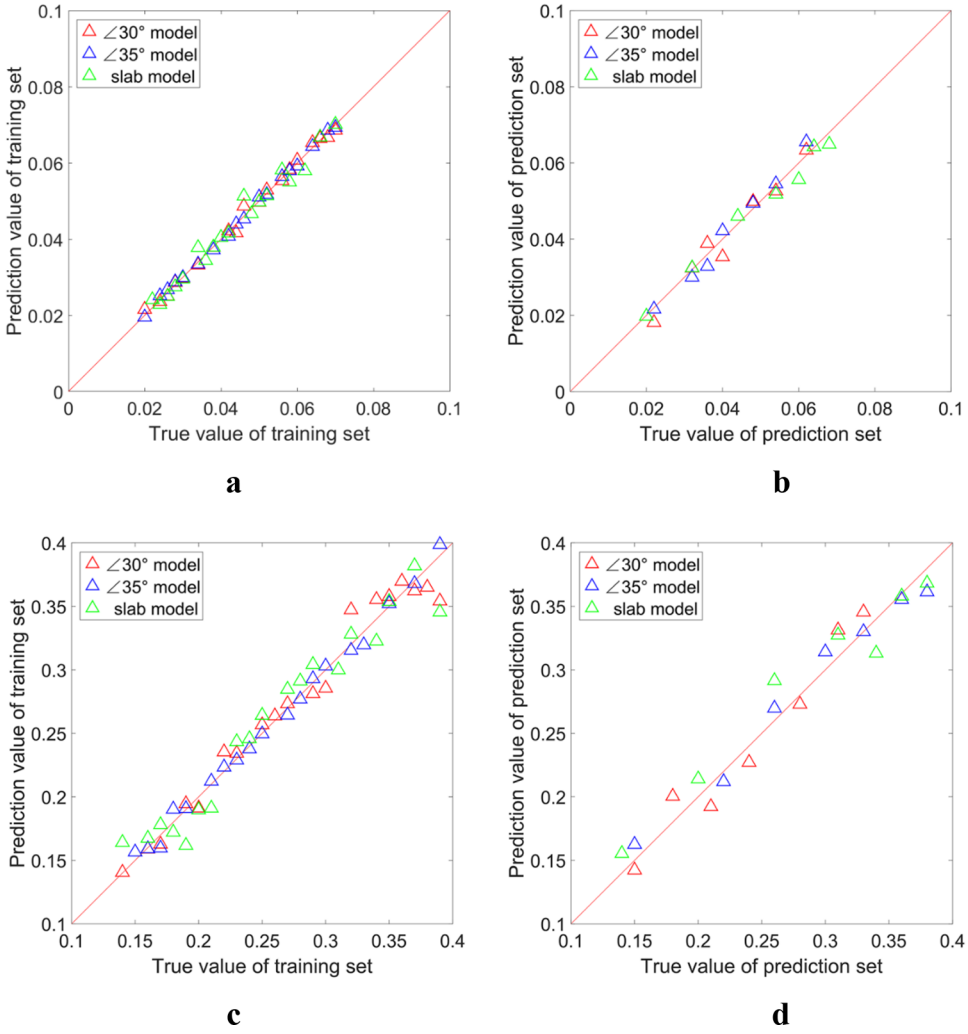

Figure 7. Comparative representation of training and prediction fitting results for scattering and absorption coefficients obtained through regression using light spot images at 30° incident angle, 35° incident angle, and flat plate models. (a) Fitting results for scattering coefficient training sets with different incident angle models. (b) Fitting results for scattering coefficient prediction sets with different incident angle models. (c) Fitting results for absorption coefficient training sets with different incident angle models. (d) Fitting results for absorption coefficient prediction sets with different incident angle models.

further validates the superiority of the 35° incident angle model in component analysis of turbid media. Additionally, it offers some insight into the stability of the model. This not only enhances the accuracy of component analysis in turbid media but also significantly improves its robustness.

The experimental results indicate that the peak shifts, differences in texture features, and dispersion levels of the light spot images obtained at a 35° incident angle more effectively reflect the scattering information in turbid media. When regressing the absorption and scattering coefficients using the light spot images obtained at a 35° incident angle, the regression coefficients also demonstrate that this incident angle significantly enhances the precision of component analysis in turbid media.

4. CONCLUSIONS

Light spot images obtained at a 35° incident angle exhibit favorable regression results when regressing the components of turbid media. Consequently, the 35° incident angle can effectively enhance the dimensionality of the optical path and photon imaging information. It better reveals the absorption and scattering information within turbid media and demonstrates a higher level of robustness. Under the 35° incident angle, optimal expression of component information within turbid media can be achieved, leading to an effective enhancement in the precision of component analysis in turbid media. This makes the rapid and accurate analysis of various components within turbid media feasible.

AUTHOR INFORMATION

Corresponding Author

Huiquan Wang − *School of Life Sciences, Tiangong University, Tianjin 300387, China; Tianjin Key Laboratory of Quality Control and Evaluation Technology for Medical Devices, Tianjin 300387, China;* orcid.org/0000-0002-7896-303X; Phone: (+86)13752356051; Email: huiquan85@126.com

Authors

Zhe Zhao − *School of Electronics and Information Engineering, Tiangong University, Tianjin 300387, China; Tianjin Key Laboratory of Quality Control and Evaluation Technology for Medical Devices, Tianjin 300387, China*

https://doi.org/10.1021/acsomega.3c09525
ACS Omega 2024, 9, 18119−18126

Ruina Zhu − *School of Life Sciences, Tiangong University, Tianjin 300387, China; Tianjin Key Laboratory of Quality Control and Evaluation Technology for Medical Devices, Tianjin 300387, China*

Yuyan Yang − *School of Electronics and Information Engineering, Tiangong University, Tianjin 300387, China; Tianjin Key Laboratory of Quality Control and Evaluation Technology for Medical Devices, Tianjin 300387, China*

Jinhai Wang − *School of Life Sciences, Tiangong University, Tianjin 300387, China; Tianjin Key Laboratory of Quality Control and Evaluation Technology for Medical Devices, Tianjin 300387, China*

Guang Han − *School of Life Sciences, Tiangong University, Tianjin 300387, China; Tianjin Key Laboratory of Quality Control and Evaluation Technology for Medical Devices, Tianjin 300387, China*

Complete contact information is available at: https://pubs.acs.org/10.1021/acsomega.3c09525

Author Contributions

The manuscript was written through contributions of all authors. All authors have given approval to the final version of the manuscript. Z.Z. provided experimental ideas and method design. R.Z. and Y.Y. collected and analyzed the data and wrote the original script. H.W. and J.W. supervised the experiment and reviewed and revised the first draft. G.H. coordinated the running of the experimental process.

Notes

The authors declare no competing financial interest.

■ ACKNOWLEDGMENTS

This work described in this paper was supported by National Natural Science Foundation of China (grant no. 62105242).

■ REFERENCES

(1) Kohl, M.; Cope, M.; Essenpreis, M.; Böcker, D. Influence of Glucose Concentration on Light Scattering in Tissue-Simulating Phantoms. *Opt. Lett.* **1994**, *19* (24), 2170−2172.

(2) Strani, L.; Grassi, S.; Alamprese, C.; Casiraghi, E.; Ghiglietti, R.; Locci, F.; Pricca, N.; De Juan, A. Effect of Physicochemical Factors and Use of Milk Powder on Milk Rennet-Coagulation: Process Understanding by near Infrared Spectroscopy and Chemometrics. *Food Control* **2021**, *119*, No. 107494.

(3) Horstmeyer, R.; Ruan, H.; Yang, C. Guidestar-Assisted Wavefront-Shaping Methods for Focusing Light into Biological Tissue. *Nat. Photonics* **2015**, *9* (9), 563−571.

(4) Zhang, S.; Li, G.; Wang, J.; Wang, D.; Han, Y.; Cao, H.; Lin, L. Nondestructive Measurement of Hemoglobin in Blood Bags Based on Multi-Pathlength VIS-NIR Spectroscopy. *Sci. Rep.* **2018**, *8* (1), 1−9.

(5) Aulbach, J.; Gjonaj, B.; Johnson, P. M.; Mosk, A. P.; Lagendijk, A. Control of Light Transmission through Opaque Scattering Media in Space and Time. *Phys. Rev. Lett.* **2011**, *106* (10), No. 103901.

(6) Zhao, Z.; Yin, H.; Yan, W.; Wang, H.; Wang, H. Investigation on Near-Infrared Quantitative Detection Based on Heteromorphic Sample Pool. *Infrared Phys. Techn.* **2019**, *97*, 444−447.

(7) Zhao, Z.; Yin, H.; Wang, Y.; Yan, W.; Wang, J.; Wang, H. Improving the Detection Accuracy of Complex Solution Components Based on Multi-Dimensional Spectroscopy Fusion Method. *Infrared Phys. Techn.* **2019**, *102*, No. 103062.

(8) Zhao, Z.; Wang, Y.; Yin, H.; Yue, C.; Wang, H.; Han, G.; Wang, J.; Miao, J.; Zhang, G.; Yu, M.; Chen, F. Research on Quantitative Analysis of Turbid Media Based on Multi-Dimension Radial Distance Method. *Infrared Phys. Techn.* **2020**, *111*, No. 103512.

(9) Yu, H.; Yan, W.; Sun, J.; Wang, H.; Zhao, Z. Study on Quantitative Detection of Turbid Solution Components Based on Ellipse Fitting. *Spectrochim. Acta Part A* **2020**, *240*, No. 118573.

(10) Tarasov, A. P.; Persheyev, S.; Rogatkin, D. A. Exact Analytical Solutions and Corresponding Monte Carlo Models for the Problem of Light Transport in Turbid Media with Continuous Absorption and Discrete Scattering at the Single Scattering Approximation. *J. Quant. Spectrosc. Radiat. Transfer* **2021**, *271*, No. 107741.

(11) Fang, Q.; Boas, D. A. Monte Carlo Simulation of Photon Migration in 3D Turbid Media Accelerated by Graphics Processing Units. *Opt. Express* **2009**, *17* (22), 20178−20190.

(12) Li, X.; Wang, Y.; Shi, G.; Lu, R.; Li, Y. Evaluation of Natural Ageing Responses on Burmese Amber Durability by FTIR Spectroscopy with PLSR and ANN Models. *Spectrochim. Acta Part A* **2023**, *285*, No. 121936.

(13) Mayr, S.; Beć, K. B.; Grabska, J.; Wiedemair, V.; Pürgy, V.; Popp, M. A.; Bonn, G. K.; Huck, C. W. Challenging Handheld NIR Spectrometers with Moisture Analysis in Plant Matrices: Performance of PLSR vs. GPR vs. ANN Modelling. *Spectrochim. Acta Part A* **2021**, *249*, No. 119342.